Biosensors and Bioelectronics 55 (2014) 120–126

Contents lists available at ScienceDirect

Biosensors and Bioelectronics

journal homepage: www.elsevier.com/locate/bios

A novel amperometric alcohol biosensor developed in a 3rd generation bioelectrode platform using peroxidase coupled ferrocene activated alcohol oxidase as biorecognition system

Somasekhar R. Chinnadayyala, Ankana Kakoti, Mallesh Santhosh, Pranab Goswami *

Department of Biotechnology, Indian Institute of Technology Guwahati, Guwahati 781039, Assam, India

ARTICLE INFO

Article history:
Received 28 September 2013
Received in revised form
28 November 2013
Accepted 1 December 2013
Available online 10 December 2013

Keywords:
Biosensor
Alcohol
Ferrocene
Alcohol oxidase
Horseradish peroxidase
Direct electron transfer

ABSTRACT

Alcohol oxidase (AOx) with a two-fold increase in efficiency (K_{cat}/K_m) was achieved by physical entrapment of the activator ferrocene in the protein matrix through a simple microwave based partial unfolding technique and was used to develop a 3rd generation biosensor for improved detection of alcohol in liquid samples. The ferrocene molecules were stably entrapped in the AOx protein matrix in a molar ratio of ~3:1 through electrostatic interaction with the Trp residues involved in the functional activity of the enzyme as demonstrated by advanced analytical techniques. The sensor was fabricated by immobilizing ferrocene entrapped alcohol oxidase (FcAOx) and sol–gel chitosan film coated horseradish peroxidase (HRP) on a multi-walled carbon nanotube (MWCNT) modified glassy carbon electrode through layer-by-layer technique. The bioelectrode reactions involved the formation of H_2O_2 by FcAOx biocatalysis of substrate alcohol followed by HRP-catalyzed reduction of the liberated H_2O_2 through MWCNT supported direct electron transfer mechanism. The amperometric biosensor exhibited a linear response to alcohol in the range of 5.0×10^{-6} to 30×10^{-4} mol L^{-1} with a detection limit of 2.3×10^{-6} mol L^{-1}, and a sensitivity of 150 μA mM^{-1} cm^{-2}. The biosensor response was steady for 28 successive measurements completed in a period of 5 h and retained ~90% of the original response even after four weeks when stored at 4 °C. The biosensor was successfully applied for the determination of alcohol in commercial samples and its performance was validated by comparing with the data obtained by GC analyses of the samples.

1. Introduction

Rapid detection of alcohol with high sensitivity and selectivity is important in food and fermentation industries, as well as in forensic and clinical analysis (Azevedo et al., 2005). The analytical techniques routinely used in industries for determination of ethanol are time consuming and labor intensive (Yildiz and Toppare, 2006). To overcome such disadvantages, a variety of alcohol biosensors based on either NAD^+ dependent alcohol dehydrogenase (ADH) (Svensson et al., 2005) or alcohol oxidase (AOx) (Patel et al., 2001) have been reported. The biosensors based on ADH usually exhibit high selectivity; however the need of supplementing the cofactor makes their use expensive (Carelli et al., 2006). The concept of using AOx (alcohol:oxygen oxidoreductases, EC 1.1.3.13) in biosensor and other industrial domains has emerged since recent past owing to many distinct properties of the enzyme identified as advantageous (Goswami et al., 2013). However, AOx based biosensors described so far are yet to address adequately the drawbacks, like low sensitivity, poor stability, and narrow linear range of operation for their practical applications. The factors responsible for these limitations are attributed to poor signal transduction, degradation or denaturation of enzyme, leaching of mediator and low loading of kinetically active enzymes on the bioelectrodes.

The common approaches utilized for transducing biochemical to electrical signal in a redox enzyme based amperometric biosensor comprises: (a) electrocatalyzed oxidation/reduction of the co-substrate or co-product such as O_2 and H_2O_2 commonly involved in the reaction, (b) utilization of electron-transfer mediators (ETM) for exchanging the electrons between the redox center of the enzyme and the electrode to generate the response. Among the various ETMs, ferrocene ($C_{10}H_{10}Fe$) and its derivatives have been widely used for developing biosensors (Qiu et al., 2008; Boguslavsky et al., 1995; Asaftei and Walder, 2004). Most biosensors available commercially are based on either of the above two approaches which, however succumb to some or all of the following drawbacks such as, low sensitivity, selectivity, reproducibility, operational stability (Vijayakumar et al., 1996) and leaching of soluble ETM from

* Corresponding author. Tel.: +91 361 2582202; fax: +91 361 2582249.
E-mail address: pgoswami@iitg.ernet.in (P. Goswami).

0956-5663/$ - see front matter © 2013 Elsevier B.V. All rights reserved.
http://dx.doi.org/10.1016/j.bios.2013.12.005

the electrode surface (Dong et al., 1992). (c) In a third approach the electrons involved in the redox process are shuttled directly between the active site of the enzyme and the electrode to generate the response (Barton et al., 2004). The key advantages credited to the biosensors based on this direct electron transfer (DET) principle are high operational stability due to mediator independent operation and interference free detection of analytes caused by the low over potential involved in the reaction. However, the major obstacle for developing a DET principle based biosensor is the deeply buried redox center in the protein of many redox enzymes that hampers the electron flow between the enzyme and the electrode. Nanofabrication of bioelectrode with highly conductive nanomaterials is emerging as a tool of choice due to its clear effect on establishing DET. In this regard MWCNT is projected as a nanomaterial of great promise as witnessed from many amperometric biosensors successfully developed in the recent past (Agui et al., 2008; Vatsyayan et al., 2011).

We developed a novel amperometric alcohol biosensor with increased sensitivity, stability and linear range of operation using AOx with enhanced biocatalytic activity on the electrode surface. The biocatalytic activity of the AOx was amplified by entrapping ferrocene, which is an activator for AOx (Kumar and Goswami, 2008), stably in the protein matrix, following a simple microwave (MW) based technique (Chinnadayyala et al., 2012). The AOx with amplified activity was immobilized on a sol–gel chitosan (SG-Chit) layer assembled on HRP in a MWCNT matrix on the electrode surface. In this bi-enzyme sensor, the H_2O_2 formed by the AOx catalyzed oxidation of alcohol was bioelectrocatalytically reduced by HRP through DET mechanism to generate the response. MWCNT provides high electroactive surface for facile electron exchange between the electrode and HRP. The silica-sol gel chitosan matrix provides biocompatible support for stability of the bi-enzyme complex on the electrode surface, desired porosity for easy diffusion of analyte and preconcentration of the analyte for electrochemical detection (Wang et al., 2003). Polyethylenimine (PEI), a polycationic polymer was used to stabilize the FcAOx immobilized on the SG-Chit film. The fabricated bioelectrode utilizing the HRP–FcAOx system has been characterized and a detailed account on response of the bioelectrode for the substrate alcohol in real samples is presented in this communication.

2. Experimental

2.1. Chemicals and reagents

AOx from *Pichia pastoris* (32 U mg^{-1} protein), peroxidase from horseradish (HRP) (1080 U mg^{-1} solid), MWCNT (OD 10–15 nm, ID 2–6 nm, length 0.1–10 μm), chitosan from crab shells ($\geq$75% deacetylated), tetraethoxysilane (TEOS), (±)-10-camphorsulfonic acid, vectaSpin microcentrifuge tube filter (20 K MWCO), ferrocene, 2,2′-azino-bis [3-ethylbenzothiazoline-6-sulfonic acid] diammonium salt (ABTS), 5% (w/v) Nafion117 in isopropanol and 50% (w/v) polyethylenimine (PEI) in water were purchased from Sigma Aldrich. Methanol, dimethyl sulphoxide, K_2HPO_4, KH_2PO_4 and 30% H_2O_2 were bought from Merck. AOx (1 mg/ml) and HRP (1 mg/ml) were freshly prepared in 50 mM potassium phosphate buffer solution (KPBS), pH 7.5 and 7.0, respectively.

2.2. Enzyme assay

The AOx activity was measured by the HRP-coupled assay method (Kemp et al., 1988). The assay was used to monitor the production of H_2O_2 at $\lambda_{405\ nm}$ for ABTS radical at 25 °C ($\varepsilon 405 = 18{,}400\ \mu M^{-1}\ cm^{-1}$). One unit of enzyme activity was expressed as the amount of enzyme required to produce 1 μM H_2O_2 min^{-1} at 25 °C.

2.3. Spectroscopic measurement

Spectrophotometric measurements were done on a Cary 300 bio UV–vis spectrophotometer (Varian) using 1 cm path length quartz cuvette at 25 °C. Fluorescence measurements were done on a Perkin Elmer LS-55 spectrofluorometer at 25 °C. Spectra, each with an average of four scans, were recorded in the scan range of $\lambda_{300\ nm}$–$\lambda_{430\ nm}$ by exciting the sample at $\lambda_{295\ nm}$ using a slit width of 5 nm and step size of 0.5 nm. The concentration of enzyme used was 0.1 mg/ml and background fluorescence was subtracted from the sample spectra.

CD spectra were recorded using a Jasco J-815 spectropolarimeter calibrated with 0.06% (w/v) aqueous solution of (±)-10-camphorsulfonic acid. The spectra were recorded from 240 to 190 nm, in a 0.1 cm path length suprasil quartz cuvette at 20 °C, a scan rate of 50 nm min^{-1} and 1 nm bandwidth. The spectra were corrected for baseline and the secondary structure analysis was performed by using DICHROWEB (Whitmore and Wallace, 2008).

2.4. Analytical ultracentrifugation

Sedimentation velocity experiments were performed with a Beckman optima XL-A/XL-I analytical ultracentrifuge equipped with absorption and interference optics. Using an An50–Ti rotor, the samples were centrifuged at 82,575*g* (20 °C). Scans were acquired at $\lambda_{280\ nm}$ and interval of 180 s. Sedimentation velocity data obtained as absorbance at $\lambda_{280\ nm}$ versus cell radius was fitted using continuous sedimentation co-efficient distribution $c(s)$ analysis with SEDFIT (Schuck, 2003), giving a residual profile in the range from −0.02 to +0.02 (Supplementary S1).

2.5. Preparation of FcAOx

A total 0.1 mg/ml of AOx (50 mM KPBS, pH 7.5) was added to 0.3 mM ferrocene at room temperature (RT). A mixture of AOx enzyme and free ferrocene was treated with MW at 2.45 GHz, 900 W for 10 s and incubated overnight at 4 °C. The refolded AOx samples in the presence of ferrocene were loaded onto Vectaspin eppendorfs, and centrifuged at 10,000*g* for 10 min. The protein retained on the membrane was washed with KPBS several times and centrifugation was repeated for removal of the residual surface bound ferrocene to collect the ferrocene entrapped AOx (FcAOx) from the membrane surface. The FcAOx was totally denatured by exposing it to MW for 1 min and then centrifuged twice at 10,000*g*. The filtrate fractions were pooled and collected for spectral analysis (Supplementary S2 A) to measure the ferrocene entrapped within the protein matrix.

2.6. Electrochemical measurements

The electrochemical measurements were done in a three-electrode system containing platinum rod as a counter electrode, Ag/AgCl as reference electrode, and GCE or modified GCE as the working electrode. All potentials were measured and reported relative to the Ag/AgCl reference electrode. During the CV measurements, the electrolyte solution was constantly purged with argon gas (99%) to maintain an anaerobic environment in the cell. Electrochemical impedance spectroscopy (EIS) measurements were performed in a background solution of 5 mM $K_3Fe(CN)_6$/$K_4Fe(CN)_6$ (1:1) and 0.1 M KCl in KPBS within the frequency range of 0.05 Hz–10 kHz. All experiments were performed at RT. The changes in the surface morphology of the bioelectrode at every step of the bioelectrode fabrication process were characterized by the field emission scanning electron microscope (FESEM) (Zeiss), with EHT 3–5 kV.

2.7. Fabrication of GCE-MWCNT-Nf-HRP-SG/Chit-FcAOx-PEI bioelectrode

GCE (diameter 0.5 cm) was cleaned by the following reported method (Das and Goswami, 2013). 3 mg of MWCNTs was dispersed in 300 μL of 5% Nf and sonicated for 20 min to obtain a stable homogenous suspension. A total 6 μL of MWCNT-Nf solution was dropped onto the GCE and allowed to dry under clean air at RT. Once dried, 5 μL of HRP from stock solution was layered above the MWCNT and dried overnight at 4 °C. Once dried, 5 μL of SG-Chit was dropped above the HRP layer and allowed to dry for 2 h under clean air at RT, and finally 5 μL of FcAOx (0.1 mg/ml) was layered over the SG-Chit layer, dried overnight at 4 °C and covered with 5 μL of 5% (v/v) PEI solution. The fabricated bioelectrode was again dried under clean air at RT and stored in KPBS at 4 °C when not in use.

3. Results and discussion

3.1. Characterization of FcAOx

The partially unfolded protein obtained by MW treatment of AOx (Chinnadayyala et al., 2012) when refolded in presence of ferrocene where the latter was entrapped within the protein matrix and generated FcAOx (shaded area in Fig. 1A). The concentration of ferrocene isolated by denaturing the FcAOx protein was determined at $\lambda_{446\ nm}$ (ε_{446}=1065 M^{-1} cm^{-1}). The molar ratio of ferrocene to AOx in FcAOx was found to be ~2.6:1.

The $c(s)$ distribution curves for native and ferrocene entrapped enzymes at 20 °C (Fig. 2A) exhibited intense major peaks, indicating non interacting homogenous systems for both enzyme fractions. The molecular weight (M_w) and sedimentation coefficients (s) of the native AOx and FcAOx were determined using a range of "s" values from 15–25s, and frictional ratio (f/f_0) of 1.2. The fit obtained yielded 'M_w' and 's' values of 575 kDa, 18.7s and 582 kDa, 19.4s for AOx and FcAOx, respectively. Increase in 'M_w' and 's' of the FcAOx by 7 kDa and 0.7s respectively, indicated stable entrapment of ferrocene molecules within the AOx protein. The molar ratio of ferrocene to AOx in FcAOx discerned from the study was 3:1.

The DPV of native AOx showed the FAD peak (I_{pa}) at −0.51 V (Munteanu et al., 2008) (Fig. 2B, curve a) and ferrocene displayed the peak at 0.23 V, characteristic for the Fe^{III} in (Fe^{III}/Fe^{II}) system (Wu et al., 2010) (Fig. 2B, curve b). FcAOx displayed a pair of peaks at −0.51 V and 0.23 V, which attribute to both FAD and ferrocene in AOx (Fig. 2B, curve c), signifying the stable entrapment of ferrocene within the protein matrix of AOx.

The CD analysis of AOx and FcAOx in KPBS validate a comparable characteristic: narrow negative peaks at 222 nm and ~208 nm, more intense positive peak at 194 nm with α-helical conformation (Chinnadayyala et al., 2012). There was no significant difference in the secondary structure composition of AOx and FcAOx (Supplementary S2B, Table S1).

The kinetic parameters for AOx were significantly improved upon addition of ferrocene in the assay mixture (Supplementary Table S2). However, the magnitude of the kinetic values was improved further when FcAOx was used instead of using a mere mixture of AOx with free ferrocene to catalyze the reaction. The Michaelis–Menten constant (K_m) and turnover number (K_{cat}) of the FcAOx were 1519 ± 31.7 μM and 0.209 ± 0.01 s^{-1}, respectively; while the corresponding values of the parameters for the native AOx with externally added ferrocene were 1869 ± 55.6 μM and 0.154 ± 0.01 s^{-1}. The K_m and K_{cat} for native AOx were 2237 ± 61.9 μM and 0.142 ± 0.01 s^{-1}, respectively. Thus, the efficiency (K_{cat}/K_m) of the AOx was increased by ~30% and ~116% by using free and entrapped ferrocene, respectively. The results confirmed that the activating role of ferrocene is facilitated by its entrapment in the AOx protein matrix. Maximum activity of the native AOx was obtained at ~0.3 mM of ferrocene (Supplementary S2 C).

The effect of salt on the activity of native AOx and FcAOx was separately studied. The activity of FcAOx decreased at elevated salt concentrations, whereas the activity of native AOx was unaltered within the salt concentration range used (Fig. 2C). The results infer that interaction between ferrocene and protein in FcAOx is electrostatic in nature, since high salt concentration is known to nullify molecular electrostatic interactions (Shields and Farrah, 1983).

The pH stability of FcAOx was studied in the pH range of 3–11 (Supplementary S3 A) and identified pH 7.5 as the optimum, which conforms to the pH stability of the native AOx. The storage stability of FcAOx in KPBS at 4 °C was studied and found that ~92% of the activity was retained at the end of 30 days of incubation of the sample (Supplementary S3 B). Successive washing of the FcAOx conjugate with KPBS even for 12 times did not alter the ferrocene concentration in the conjugate.

A study was conducted to identify the amino acid residue (s) that electrostatically hold the ferrocene molecule in the AOx protein matrix. Ferrocene strongly quenched the Trp fluorescence

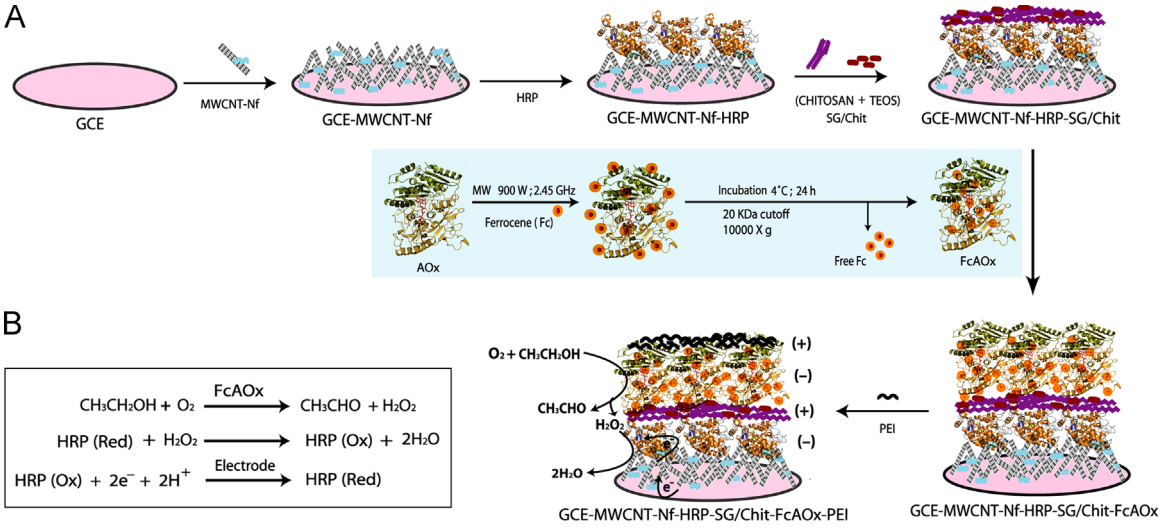

Fig. 1. (A) Schematic depiction of the bienzyme electrode fabrication process. (B) The principal reactions catalyzed by FcAOx and HRP at electrode surface.

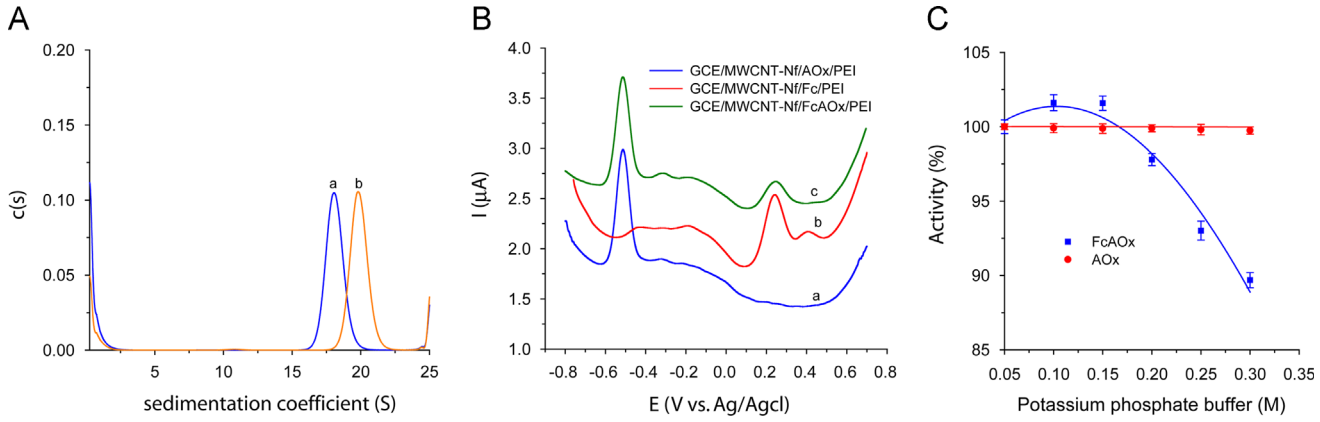

Fig. 2. (A) Continuous sedimentation co-efficient $c(s)$ distribution analysis of the simulated data from sedimentation velocity experiment showing 's' values for (a) AOx and (b) FcAOx fitted using the parameters $\acute{\nu}$=0.73 mL/g and ρ=1.00 g/cm^3. (B) DPV of differently modified electrodes showing (a) GCE-MWCNT-Nf-AOx-PEI, (b) GCE-MWCNT-Nf-Fc-PEI and, (c) GCE-MWCNT-Nf-FcAOx-PEI. (C) FcAOx activity as a function of ionic strength as salt concentration of potassium phosphate buffer (pH 7.5).

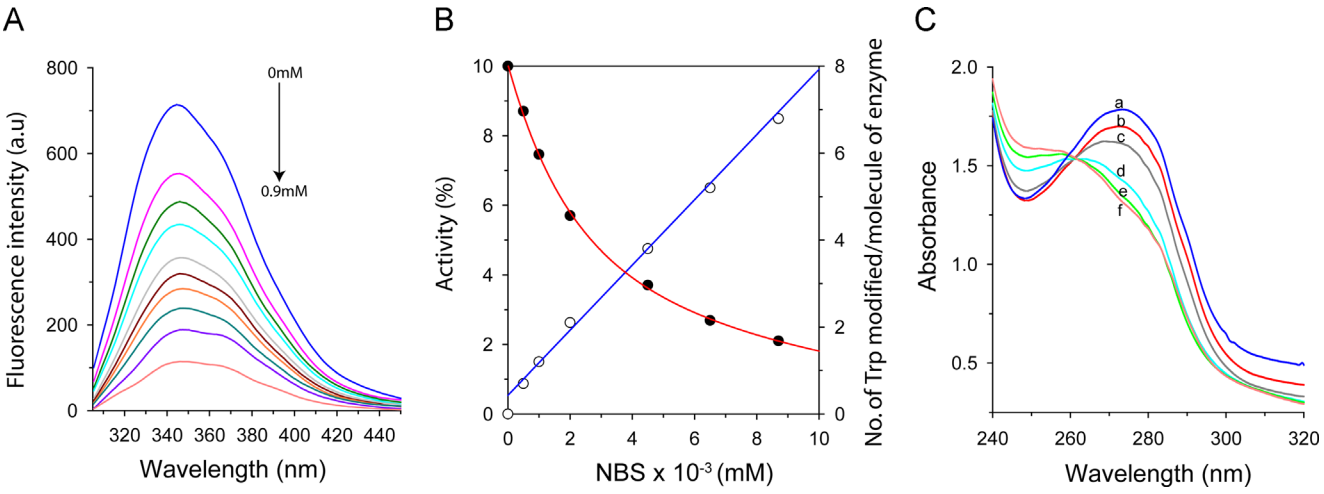

Fig. 3. (A) Trp fluorescence emission spectra of AOx when mixed with different concentrations of ferrocene in a 0.1 mM gradient as indicated by the arrow line. (B) AOx activity versus NBS concentration involved in the oxidative blocking of Trp residues. The number of Trp residues oxidized was calculated from the decrease in absorbance at $\lambda_{278\ nm}$. (C) Absorption spectra of native (a) and NBS modified AOx (b, c, d, e, and f). Enzyme concentration was 14 μM in 0.1 M sodium acetate buffer, pH 4.0. The test volume was 1.0 mL.

intensity (emission at $\lambda_{344\ nm}$, excitation at $\lambda_{295\ nm}$) of AOx protein in a concentration dependent manner (Fig. 3A). The quenching effect was increased linearly at a rate of 5.82 au s^{-1} with MW treatment time, indicating the enhanced interaction of ferrocene molecules with the exposed Trp residues in the gradually unfolded AOx protein (Supplementary S4 A). Furthermore, Trp residue (s) are involved in the catalytic activity of AOx as evident from the loss of more than 50% of the enzyme activity when as many as three Trp residues were modified by N-bromosuccinimide (NBS) (Fig. 3B). The nature of the isobestic point at $\lambda_{263\ nm}$ (Fig. 3C) and decrease in the Trp fluorescence intensity (Supplementary S4 B) infers that the loss of activity is due to Trp modification rather than structural changes or modification of tyrosine residues (Paus, 1978). The results signify that a maximum of three Trp residues play a critical role in the enzyme activity. It is likely that the ferrocene molecules are retained in the protein matrix by the Trp residues through pi-stacking interactions between the indolic ring of Trp and the cyclopentadienyl rings of ferrocene and thereby accelerating the catalytic activity of the AOx. Pi stacking is known to contribute to the interactions between small aromatic molecules and proteins (Babine and Bender, 1997). However, to understand the exact role of ferrocene and its interaction with the Trp residues on the activity of AOx, the active site configuration of the AOx needs to be elucidated, which is however beyond the scope of this communication and will be dealt with separately when the X-ray crystallography data on *Pichia pastoris* AOx will be available.

3.2. Characterization of bioelectrode

The smooth bare GCE surface (Supplementary S5 A) transformed into a porous thread like morphology when MWCNTs was layered on it (Fig. 4A). The porous nature of the layer was diminished upon addition of HRP on the film (Supplementary S5 B). When a layer of SG-Chit was applied on the film to fabricate the GCE-MWCNT-Nf-HRP-SG/Chit bioelectrode, the surface morphology changed to an uneven form with a rough surface (Supplementary S5 C), which provides an effective electrode surface area for increased immobilization of biomolecules. The surface of the GCE-MWCNT-Nf-HRP-SG/Chit electrode changes to globular morphology after immobilization of FcAOx revealing successful immobilization of the enzyme (Fig. 4B). Finally when a layer of PEI was applied on the GCE-MWCNT-Nf-HRP-SG/Chit-FcAOx film, the surface morphology changed to smooth even form (Fig. 4C). Stability of the immobilized layers on the electrode surface occurred under the influence of electrostatic interaction between the negatively and positively charged layers in the electrode surface as shown schematically in Fig. 1A. CV of bare GCE and modified GCE was done in an argon-saturated KPBS

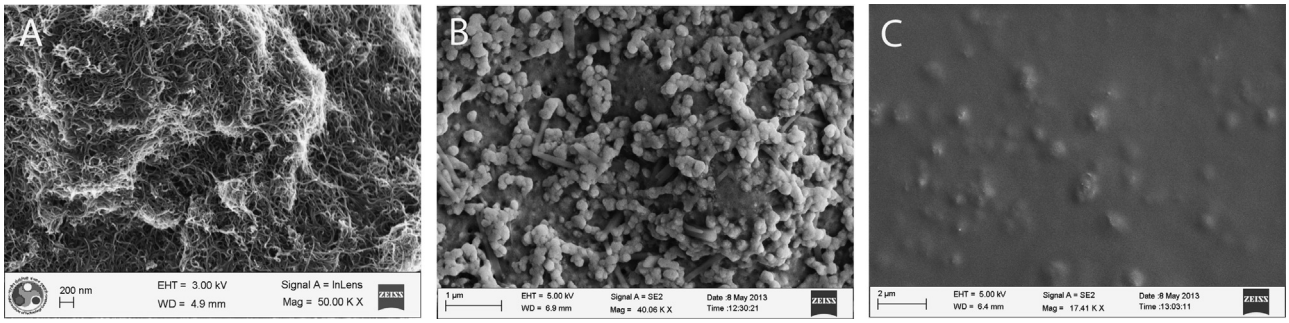

Fig. 4. FESEM images of (A) GCE-MWCNT-Nf, (B) GCE-MWCNT-Nf-HRP-SG/Chit-FcAOx, (C) GCE-MWCNT-Nf-HRP-SG/Chit-FcAOx-PEI with EHT 3–5 kV.

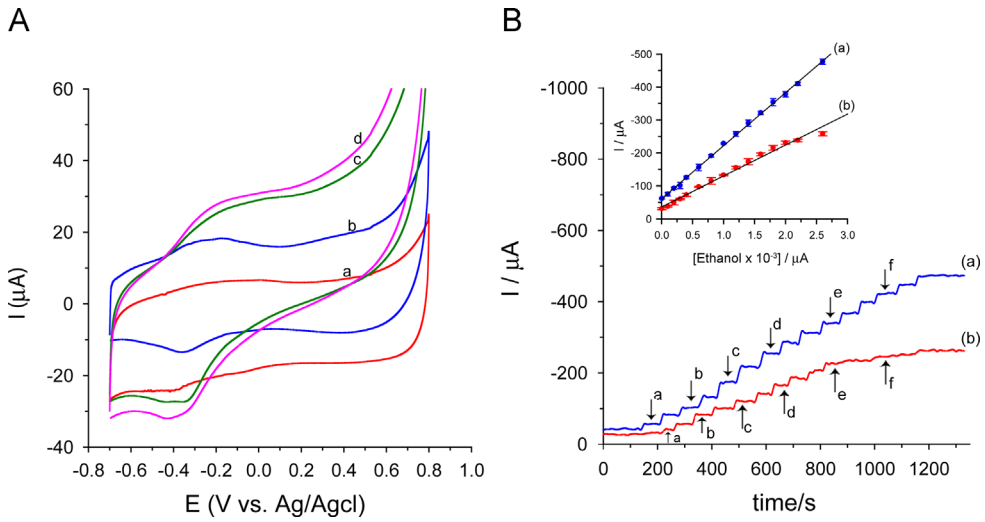

Fig. 5. (A) CV of background current subtracted electrodes: (a) GCE-MWCNT-Nf, (b) GCE-MWCNT-Nf-HRP-SG/Chit, (c) GCE-MWCNT-Nf-HRP-SG/Chit-FcAOx-PEI, (d) GCE-MWCNT-Nf-HRP-SG/Chit-FcAOx-PEI with 5 µM ethanol in an argon gas purged solution of 50 mM KPBS (pH 7.5) at a scan rate of 50 mV s^{-1}. (B) Chronoamperometric current responses of the GCE-MWCNT-Nf-HRP-SG/Chit-FcAOx-PEI (a) and GCE-MWCNT-Nf-HRP-SG/Chit-AOx-PEI (b) bioelectrodes for successive addition of alcohol (a) 5 µM, (b) 50 µM, (c) 100 µM, (d) 500 µM, (e) 1000 µM and (f) 3000 µM. Inset of Fig. 5B: response curves of the bioelectrodes (a) GCE-MWCNT-Nf-HRP-SG/Chit-FcAOx-PEI, (b) GCE-MWCNT-Nf-HRP-SG/Chit-AOx-PEI with increasing ethanol concentration in argon purged solution of KPBS. The operating potential used was −0.34 V (vs. Ag/AgCl electrode). (For interpretation of the references to color in this figure, the reader is referred to the web version of this article.)

(50 mM, pH 7.5) at 50 mV s^{-1} (Fig. 5A). No clear redox peaks were observed for bare GCE and GCE-MWCNT-Nf (Fig. 5A, curve a) suggesting that the MWCNT-Nf layer is electro-inactive in this potential window. The GCE-MWCNT-Nf-HRP-SG/Chit bioelectrode generated by immobilization of HRP and SG-Chit on the MWCNT-Nf film displayed a pair of redox peaks at −0.23 V and −0.34 V, which are characteristic for the direct electrochemistry of HRP (Zhao et al., 2008) (Fig. 5A, curve b). Following the immobilization of FcAOx and PEI over the GCE-MWCNT-Nf-HRP-SG/Chit film, the generated bioelectrode (Fig. 5A, curve c) displayed a pair of redox peaks similar to that of curve b with increased peak currents. The formal potential $[(E_{pa}+E_{pc})/2]$ of the redox couple at bioelectrode GCE-MWCNT-Nf-HRP-SG/Chit-FcAOx-PEI was −0.28, which is nearly conforming to the previous reports for HRP (Fe^{III}/Fe^{II}) on direct electrochemistry (Xu et al., 2006). The magnitude of cathodic peak current was significantly higher than the corresponding anodic peak current in presence of alcohol (Fig. 5A, curve d). The H_2O_2 produced by the FcAOx catalyzed oxidation of alcohol could be biocatalytically reduced by the HRP leading to the formation of HRP (Ox), which in turn electrocatalytically reduced at −0.34 V to HRP (red) on the electrode surface through DET mechanism and regenerated the reaction for the next cycle as depicted in Fig. 1 B. The increased cathodic peak current was further validated by the chronoamperometric response of the bioelectrode for alcohol at −0.34 V as described below.

The EIS was performed to validate the formation of different layers on the electrode surface (Supplementary S6). The bare GCE exhibits a line with small semicircle diameter with R_{ct} (charge-transfer resistance) of 140 Ω (curve a). The semicircle disappeared upon layering of MWCNT onto the GCE, implying that a highly conductive MWCNT film facilitates the charge transfer with the electrode (curve b). Reappearance of a semicircle line with R_{ct} of 311 Ω (curve c) upon layering of HRP/SG-Chit on the MWCNT-Nf film indicates the formation of the HRP/SG-Chit film that reduces the charge transfer on the electrode surface. The R_{ct} of the GCE-MWCNT-Nf-HRP-SG/Chit electrode was further increased to 390 and 410 Ω (curve d) when FcAOx/AOx and PEI were stepwise layered on it, indicating the formation of these successive layers with increasing charge transfer resistance on the electrode surface.

The optimum pH 7.5 identified for the bioelectrode response conformed to the pH optimum for biocatalytic reaction of AOx (Suye, 1997). Fig. 5B illustrates a typical current–time plot (at −0.34 V) on successive step addition of alcohol dose. The magnitude of the cathodic current was increased linearly with increasing ethanol concentration and reached saturation at 3000 µM of ethanol for the FcAOx bioelectrode (inset of Fig. 5B, curve a) and 1800 µM for the AOx bioelectrode (inset of Fig. 5B, curve b). The response characteristics obtained from the FcAOx based bioelectrode were compared with those obtained from the AOx-based bioelectrode and observed that all the response characteristics were substantially improved when FcAOx was used in the bioelectrode (Table 1). The biosensor responses for various alcohols (each at 0.05 mM) were tested. Considering the activity on methanol as 100%, the activity on ethanol (71%), 1-propanol (<9.2%), 1-butanol (<1%) and benzyl alcohol

Table 1
Response characteristics of the bienzyme bioelectrode based biosensor.

Response characteristics	Bioelectrode	
	GCE-MWCNT-Nf-HRP-SG/Chit-FcAOx-PEI	GCE-MWCNT-Nf-HRP-SG/Chit-AOx-PEI
Linear range (μM)	5–3000	5–1800
Correlation co-efficient, *r*	0.9976	0.9951
Detection limit (*DL*)[a] (μM)	2.32 ± 0.018	4.61 ± 0.050
Sensitivity (μA mM^{-1} cm^{-2})	150 ± 0.25	90 ± 0.31
Standard deviation (*SD*) limit (μA)	0.117 ± 0.02	0.140 ± 0.05
Response time (*s*)	20	35

[a] $DL = (3 \times SD)$/Sensitivity (where *SD* is the estimated standard deviation for the points used to construct the calibration curve and the Sensitivity, its slope).

(< 1%) were recorded and as expected, the current response decreased with increasing aliphatic chain length of the alcohol molecule.

A comparative analysis on the performance of various prominent 1st (Lee and Tsai, 2009; Patel et al., 2001), 2nd (de Parda et al., 2003; Hasunuma et al., 2004; Smutok et al., 2006; Gouveia-Caridade et al., 2008; Jimenez et al., 2013; Manso et al., 2008; Tsai et al., 2007) and 3rd generation (Das and Goswami, 2013) alcohol biosensors reported so far showed that the present FcAOx based biosensor offers improved operational stability, wide linear range of response with lower minimum concentration in the range, and improved detection limit. The ADH based biosensor (Lee and Tsai, 2009) though showed marginally higher sensitivity of 164.6 μA mM^{-1} cm^{-2}, the other critical performances namely, stability, detection limit and linear range obtained by the present biosensor are improved. The cause of improved detection limit and sensitivity of the FcAOx based biosensor is ascribed to the amplified activity of the AOx obtained by entrapping the activator ferrocene in it and the DET mechanism involved in the signal transduction of the biosensor. The improved kinetic parameters, such as lower K_m value of the FcAOx substantially contributed to the aforementioned improved functional activities of the biosensor as evident from the comparative analysis of the performance with a native AOx based biosensor shown in Table 1. The electrostatic interaction principle utilized by us for the physical immobilization of the enzyme on the biocompatible chitosan-sol–gel-based electrode surface provided a significant operational stability and reproducibility on the response of the biosensor.

3.3. Stability and interference studies

The operational stability of the electrode was investigated for 28 successive measurements with 3 mM of alcohol (the highest response in the linear range) during a period of 5 h. Our results demonstrated that the bioelectrode still maintained 90% of its initial activity at the end of 28 measurements (Supplementary S7 A). The reproducibility of the bioelectrode was estimated from the response to various alcohol concentrations at three bioelectrodes prepared by similar procedure. The results showed the acceptable reproducibility with a relative standard deviation (RSD) of ~2% for the bioelectrode. The storage stability of the bioelectrode was examined by carrying out the response measurements at a regular interval of 3 days and found that the bioelectrode retains ~90% of the original response even after five weeks when stored at 4 °C and pH 7.5 (Supplementary S7 B). The half-life ($t_{1/2}$) of the biosensors under the above storage condition was ~184 days. To study the selectivity of the sensor towards alcohol, the effect of some potential interfering agents present in real samples namely, ascorbic acid, lactic acid, glucose, urea and uric acid, on biosensor response was studied in 50 mM KPBS (pH 7.5) at −0.34 V. The response of the sensor was examined by exposing it separately to these interferents, with analyte in 1:1 ratio (Supplementary S7 C). The selectivity co-efficient (SC) of ~1 for each interferent estimated using the formula, $SC = I_{c+i}/I_c$, where I_{c+i} and I_c are response for alcohol in the presence and absence of each interferents, respectively infers that these compounds did not significantly affect the biosensor response.

3.4. Analysis of commercial alcohol samples

The ethanol content (mg/mL) in three different beer samples (A, B, and C) was determined (at −0.34 V) using the GCE-MWCNT-Nf-HRP-SG/Chit-FcAOx-PEI biosensor by the multiple standard addition method without any pretreatment of the samples and found to be 0.39 ± 0.014, 0.43 ± 0.021 and 0.41 ± 0.017 for sample A, B and C, respectively. The concentrations of ethanol in the same samples were also measured by gas chromatography and found to be 0.41 ± 0.016, 0.44 ± 0.015 and 0.40 ± 0.012 for the samples A, B, and C, respectively. The comparison of the data was done by paired *t*-test (Sigma 11) and no significant differences were found ($P = 0.709$) between the results obtained by the methods. The study validates the reliability of the existing biosensor for sensitive and quantitative analysis of industrial samples.

4. Conclusions

Stable entrapment of chemical activator in the protein matrix for enhancing biocatalytic activity of an enzyme has been reported here for the first time through entrapment of activator ferrocene in the AOx protein. The amplified biocatalytic activity of AOx has been exploited to develop an efficient biosensor using direct electrochemistry as the governing principle for selective interference free detection of alcohol in real sample. The overall performance of the fabricated biosensor improved as compared to the previously reported biosensors for detection of alcohol in liquid sample. The constructed biosensor exhibited good correlation with the standard analytical method, suggesting its application potential in alcohol industries.

Acknowledgments

Financial assistance from DBT, India and the FESEM facility from CIF, IITG to carry out this work are acknowledged. We are thankful to Prof. John W. Burgner, Purdue University for helping in analyzing the analytical ultracentrifugation data.

Appendix A. Supporting information

Supplementary data associated with this article can be found in the online version at http://dx.doi.org/10.1016/j.bios.2013.12.005

References

Agui, L., Yanez-Sedeno, P., Pingarron, J.M., 2008. Anal. Chim. Acta 622, 11–47.
Asaftei, S., Walder, L., 2004. Electrochim. Acta 49, 4679–4685.
Azevedo, A.M., Prazeres, D.M.F., Cabral, J.M.S., Fonseca, L.P., 2005. Biosens. Bioelectron. 21, 235–247.
Babine, R.E., Bender, S.L., 1997. Chem. Rev. 97, 1359–1472.
Barton, S.C., Gallaway, J., Atanassov, P., 2004. Chem. Rev. 104, 4867–4886.
Boguslavsky, L., Kalash, H., Xu, Z., Beckles, D., Geng, L., Skotheim, T., Laurinavicius, V., Lee, H.S., 1995. Anal. Chim. Acta 311, 15–21.
Carelli, D., Centonze, D., Giglio, A.D., Quinto, M., 2006. Anal. Chim. Acta 565, 27–35.
Chinnadayyala, S.S.R., Santhosh, M., Goswami, P., 2012. J. Biophys. Chem. 3, 317–323.

Das, M., Goswami, P., 2013. Bioelectrochemistry 89, 19–25.
de Parda, G.V.A., Pena, N., Mena, M.L., Reviejo, A.J., Pingarron, J.M., 2003. Biosens. Bioelectron. 18, 1279–1288.
Dong, S., Wang, B., Liu, B., 1992. Biosens. Bioelectron. 7, 215–222.
Goswami, P., Chinnadayyala, S.S.R., Chakraborty, M., Kumar, A.K., Kakoti, A., 2013. Appl. Microbiol. Biotechnol. 97, 4259–4275.
Gouveia-Caridade, C., Pauliukaite, R., Brett, C.M.A., 2008. Electrochim. Acta 53, 6732–6739.
Hasunuma, T., Kuwabata, S., Fukusaki, E., Kobayashi, A., 2004. Anal. Chem. 76, 1500–1506.
Jimenez, A., Armada, M.P.G., Losada, J., Villena, C., Alonso, B., Casado, C.M., 2014. Sens. Actuators B 190, 111–119.
Kemp, G.D., Dickinson, F.M., Ratledge, C., 1988. Appl. Microbiol. Biotechnol. 29, 370–374.
Kumar, A.K., Goswami, P., 2008. Biochim. Biophys. Acta 1784, 1552–1559.
Lee, A.N., Tsai, Y.C., 2009. Sens. Actuators B 138, 518–523.
Manso, J., Mena, M.L., Yanez-Sedeno, P., Pingarron, J.M., 2008. Electrochim. Acta 53, 4007–4012.
Munteanu, F.D., Ferreira, P., Ruiz-Duenas, F.J., Martinez, A.T., Cavaco-Paulo, A., 2008. J. Electroanal. Chem. 618, 83–86.
Patel, N.G., Meier, S., Cammann, K., Chemnitius, G.-C., 2001. Sens. Actuators B 75, 101–110.
Paus, E., 1978. Biochim. Biophys. Acta 533, 446–456.
Qiu, J.-D., Deng, M.-Q., Liang, R.-P., Xiong, M., 2008. Sens. Actuators B 135, 181–187.
Schuck, P., 2003. Anal. Biochem. 320, 104–124.
Shields, P.A., Farrah, S.R., 1983. Appl. Environ. Microbiol. 45, 526–531.
Smutok, O., Ngounou, B., Pavlishko, H., Gayda, G., Gonchar, M., Schuhmann, W., 2006. Sens. Actuators B 113, 590–598.
Suye, S., 1997. Curr. Microbiol. 34, 374–377.
Svensson, K., Bulow, L., Kriz, D., Krook, M., 2005. Biosens. Bioelectron. 21, 705–711.
Tsai, Y.-C., Huang, J.-D., Chiu, C.-C., 2007. Biosens. Bioelectron. 22, 3051–3056.
Vatsyayan, P., Chakraborty, M., Bordoloi, S., Goswami, P., 2011. J. Electroanal. Chem. 662, 312–316.
Vijayakumar, A.R., Csoregi, E., Heller, A., Gorton, L., 1996. Anal. Chim. Acta 327, 223–234.
Wang, G., Xu, J.J., Chen, H.Y., Lu, Z.H., 2003. Biosens. Bioelectron. 18, 335–343.
Whitmore, L., Wallace, B.A., 2008. Biopolymers 89, 392–400.
Wu, J., Fu, Q., Lu, B., Li, H., Xu, Z., 2010. Thin Solid Films 518, 3240–3245.
Xu, Q., Mao, C., Liu, N.N., Zhu, J.J., Sheng, J., 2006. Biosens. Bioelectron. 22, 768–773.
Yildiz, H.B., Toppare, L., 2006. Biosens. Bioelectron. 21, 2306–2310.
Zhao, X., Mai, Z., Kang, X., Zou, X., 2008. Biosens. Bioelectron. 23, 1032–1038.